Chemical Engineering Science 64 (2009) 2433 – 2447

Contents lists available at ScienceDirect

Chemical Engineering Science

journal homepage: www.elsevier.com/locate/ces

Experimental studies and population balance equation models for breakage prediction of emulsion drop size distributions

Neha B. Raikar, Surita R. Bhatia, Michael F. Malone, Michael A. Henson*

Department of Chemical Engineering, University of Massachusetts, Amherst, MA 01003-9303, USA

ARTICLE INFO

Article history:
Received 21 July 2008
Received in revised form 10 January 2009
Accepted 27 January 2009
Available online 14 February 2009

Keywords:
Emulsions
Drop breakage
Drop size distributions
Population balance equation models
Parameter estimation

ABSTRACT

A population balance equation (PBE) model for pure drop breakage processes was developed from homogenization experiments and used to investigate model extensibility over a range of emulsion formulation and homogenizer operating variables. Adjustable parameters in the mechanistic breakage functions were estimated from measured drop volume distributions by constrained nonlinear least-squares optimization. Satisfactory prediction of measured bimodal distributions was achieved by the incorporation of two different breakage functions that accounted for large drop breakage due to turbulent shear and for small drop breakage due to collisions between drops and turbulent eddies. Model extensibility to different emulsion compositions and homogenizer pressures was investigated by comparing model predictions generated with the base case parameters to drop volume distributions measured under different conditions. The PBE model satisfactorily accounted for changes in the dispersed phase volume fraction and the interfacial tension with the base case parameters. By contrast, significantly improved predictions for the continuous phase viscosity or multiple formulation variables were obtained through re-estimation of the model parameters using multiple data sets in which the associated variables were systematically varied. The model was not able to satisfactorily predict drop volume distributions resulting from homogenizer pressure changes, perhaps due to the assumption of a constant pressure throughout the homogenizer. We conclude that PBE models of drop breakage can be used to reasonably predict the effects of emulsion formulation variables on drop volume distributions and have the potential for guiding experimental efforts aimed at the design of novel emulsified products.

1. Introduction

Oil-in-water emulsions are ubiquitous in petroleum-based consumer products, including cosmetics, creams, lotions, and agricultural products (Chappat, 1994; Israelachvili, 1994). Emulsions are also encountered throughout the petroleum industry with applications at many stages of petroleum recovery, transportation, and processing (Becher, 2001; Schramm, 1992). In petroleum recovery applications, emulsion formation at the well-head is undesirable while emulsions are critical for enhanced oil recovery as drilling muds and fluids. Heavy crude oils typically have viscosities in the range of a few hundred to several thousand centipoise, and therefore they cannot be transported economically in conventional pipelines without reducing their viscosity (Nasr-El-Din, 1992). Emulsifying heavy oils with an aqueous solution significantly reduces the viscosity, allowing for lower pumping power requirements and more economical transportation (Saniere et al., 2004; Rimmer et al., 1992; Yaghi and Al-Bemani, 2002).

The emulsion drop size distribution has a significant effect on emulsion stability as well as on emulsion viscosity, and hence pipeline frictional losses and pumping power. For petroleum applications, emulsions with small drops are desirable to promote stability and minimize viscosity (Nasr-El-Din, 1992; Pal et al., 1992). Coarse emulsions are typically formed by low-shear mixing in an agitated vessel, followed by a high-shear process to create smaller drops. The prepared emulsions are then stored under static conditions before introduction into the pipeline (Schramm, 1992; Rimmer et al., 1992). Drop breakage and coalescence during high-shear preparation have a substantial impacts on the drop size distribution. While drop breakage under laminar conditions has been extensively studied (Dhingra, 2001; Gupta, 2004), predictive models for drop breakage and coalescence under turbulent conditions are lacking.

Due the lack of suitable models, emulsified products are currently developed by combining a broad knowledge of the previous product formulations with empirical scientific experimentation to create new formulations with desired properties. Because this approach is

* Corresponding author. Tel.: +1 413 545 3481; fax: +1 413 545 1647.
E-mail address: henson@ecs.umass.edu (Michael A. Henson).

0009-2509/$ - see front matter © 2009 Elsevier Ltd. All rights reserved.
doi:10.1016/j.ces.2009.01.062

intuitive and experimental, the progression of a formulation is generally unpredictable and a new product will often go through hundreds of prototype formulations in a laboratory or pilot plant before commercialization. Due to the very large number of possible formulation and processing combinations that need to be explored, the traditional trial-and-error approach requires significant time and resources. The lack of suitable models has impeded the development of systematic methodologies for designing emulsified products. Such methodologies will not eliminate the need for laboratory experimentation, but rather they will serve to guide and focus product experimentation on quantifying key physicochemical properties instead of attempting to directly identify new product formulations.

Population balance equation (PBE) models have been widely used to predict drop size distributions in turbulently agitated liquid–liquid dispersions (Ramkrishna, 2000). More recently, several investigators have developed PBE models of high pressure homogenizers for the preparation of oil-in-water emulsions (Floury et al., 2004a,b; Soon et al., 2001; Vankova et al., 2007ab). The key challenge associated with the formulation of predictive PBE models is experimental determination of unknown drop breakage and coalescence functions. In this paper, we restrict our analysis to pure breakage processes under the assumption of negligible drop coalescence. A volume-structured PBE model includes three breakage functions for the breakage rate $g(v)$, the number $\nu(v)$ of daughter drops formed from breakage of a mother drop, and the probability $\beta(v, v')$ of obtaining daughter drops of size v from breakage of mother drops of volume v'. To avoid complications associated with modeling multiple daughter drop formation, binary breakage is commonly assumed such that $\nu(v) = 2$. While several functional forms have been proposed for the probability $\beta(v, v')$, available functions are phenomenological rather than based on fundamental principles (Alopaeus et al., 2002; Coulaloglou and Tavlarides, 1977; Ruiz and Padilla, 2004; Tcholakova et al., 2007). By contrast, mechanistic modeling of the breakage rate $g(v)$ has received considerable attention and a variety of functional forms are available (Chen et al., 1998; Coulaloglou and Tavlarides, 1977).

From a product engineering perspective, mechanistic breakage rate functions that depend on the emulsion chemical formulation (oil, water, and surfactant concentrations) through bulk physical properties (dispersed phase volume fraction, continuous phase viscosity, and interfacial tension) are preferred to empirical forms such as power law functions obtained through inverse PBE modeling (Ramkrishna, 2000; Raikar et al., 2006; Sathyagal et al., 1995; Sathyagal and Ramkrishna, 1996). In principle, mechanistic breakage functions can be identified from limited experimental data for a particular chemical formulation and then used to predict drop volume distributions that result from different chemical compositions. From a process engineering perspective, the breakage rate should also depend on emulsification equipment parameters, such as the stirrer speed of an agitated vessel or the operating pressure of a homogenizer, to allow prediction of drop volume distributions that result from different process operating conditions. This connection can be made through process-specific expressions for the energy dissipation rate that commonly appears in mechanistic breakage rate functions (Chen et al., 1998; Floury et al., 2004b). Surprisingly, we have not found any studies in which PBE model extensibility to different chemical compositions or process conditions has been tested experimentally.

In this paper, we develop a PBE model for pure drop breakage processes by fitting model parameters to data collected from high-pressure homogenization experiments and evaluate model extensibility over a range of emulsion formulation and homogenizer operating variables. Homogenizer flow regimes are investigated using computational fluid dynamics (CFD) to better understand relevant drop breakage mechanisms and to motivate development of two mechanistic breakage functions. Nonlinear least-squares optimization is used to estimate adjustable parameters in breakage rate functions from measured drop volume distributions. Model extensibility is evaluated by comparing predictions generated with the base case parameters to drop volume distributions measured for different dispersed phase volume fractions, interfacial tensions, continuous phase viscosities, and homogenizer pressures.

2. Experimental methods

2.1. Materials

We used soybean oil (Spectrum Organic) as the dispersed phase, nanopure water as the continuous phase, and the nonionic surfactant Pluronic F-68 (Sigma Aldrich) as the emulsifier. The base case emulsion consisted of 0.5 wt% oil and 0.1 wt% surfactant with the remainder water (Table 1). Relatively low oil and high surfactant concentrations were used to minimize the possibility of coalescence, an assumption tested experimentally through a specific coalescence experiment (see Section 4.2). Emulsions were prepared at concentrations different than the base case listed in Table 2 to test extensibility of the PBE model for varying bulk emulsion properties. The dispersed phase volume fraction was changed by adjusting the amount of oil, and the interfacial tension was changed by adjusting the amount of surfactant. To change the continuous phase viscosity, varying amounts of sucrose (Fisher Scientific) were added to the nanopure water.

2.2. Emulsion preparation

Emulsions were prepared using a two-step process. First about 100 ml of coarse pre-emulsion was prepared by mixing the chemical ingredients in a stator–rotor device (Ultra-Turrax Model T25, Rose Scientific Ltd.) at 13 000 rpm for 1 min (Table 1). Approximately 5 ml of the pre-emulsion was sampled for measuring the drop size distribution (see below). The pre-emulsion was then processed in a high-pressure homogenizer (Emulsiflex C-3, Avestin Inc.) where the liquid was pressurized to 10 000 psig (68.95 MPa) and then expanded through a narrow valve gap to create turbulent shear conditions favoring drop breakage. Multiple passes each approximately 2 min long were performed by reprocessing the emulsion obtained from the previous homogenizer pass. Five passes were performed for each experiment, and after each pass 5 ml of the emulsion was sampled for drop size distribution measurement. Experiments were also performed at different pressures (5000–20 000 Psig) than the base case value to test extensibility of the PBE model (Table 2).

Table 1
Base case emulsion formulation and homogenization values.

Soybean oil	0.5 wt%
Pluronic F-68	0.1 wt%
Dispersed phase volume fraction (ϕ)	5.59×10^{-3}
Interfacial tension (σ)	13.68 mN/m
Continuous phase viscosity (η_c)	1 cP
Homogenizer pressure (P)	10000 psig (68.95 MPa)

Table 2
Range of emulsion formulations and homogenization pressures studied.

Dispersed phase volume fraction (ϕ)	2.78×10^{-3} to 0.0228
Interfacial tension (σ)	14.318–12.68 mN/m
Continuous phase viscosity (η_c)	1–1.3 cP
Homogenizer pressure (P)	5000–20 000 psig (34.48–137.9 MPa)

2.3. Emulsion characterization

Drop size distributions were measured using a static light scattering device (Coulter LS230 Particle Size Analyzer, Beckman Coulter). Optical microscopy (Olympus IX71 Inverted Microscope, Olympus) at a magnification of 20× and 40× was used to visually analyze drop sizes. Oil–water interfacial tensions were measured by drop shape analysis (KRUSS Instruments Model DSA-10 Tensiometer, KRUSS) at 25 °C. Continuous and dispersed phase viscosities were measured using a Ubbelohde type capillary viscometer (Model CT-1000, Canon Instruments Company) at 25 °C. We found that large amounts of added sucrose designed to vary the continuous phase viscosity also slightly changed the interfacial tension. This issue is discussed further in the results section.

3. Theory

3.1. Computational fluid dynamics (CFD)

A CFD study was performed to better understand the flow field near the homogenizer valve. Because our goal was to identify possible turbulent mechanisms for drop breakage rather than to model the effects of inhomogeneous flow fields on drop breakage, the CFD computations were performed separately from the PBE model solution. The interested reader is referred elsewhere for CFD studies in which the PBE model is coupled to the flow field calculations (Dorao and Jakobsen, 2006; Gavi et al., 2008; Jaworski et al., 2007; Kim and Kramer, 2006; Woo et al., 2006).

Because our intention was to analyze bulk flow fields and not to track droplets, only continuous phase properties were considered under the assumption that the flow properties of our very dilute emulsions were dictated by the continuous phase fluid (water). The CFD analysis was restricted to a two-dimensional axisymmetric representation of the homogenizer valve near the narrow gap shown in Fig. 3 (Kelly and Muske, 2004; Lander et al., 2000; Miller et al., 2002). The geometry was meshed using Gambit v2.2.30, and the flow field calculations were performed using Fluent v6.2.16 (Guide, 2005). Interactions between the water liquid and vapor phases were captured using the Fluent cavitation model. The standard k–ε model was used for turbulence with no-slip boundary condition at the walls, and pressure-velocity coupling was captured using the SIMPLEC algorithm. A constant velocity of 0.42 m s^{-1} calculated from the homogenizer flow rate and the valve gap was introduced normal to the inlet plane, and the outlet pressure was set to 950 psig (6.5 MPa) since only a truncated section of the homogenizer was considered. The numerical solution was considered converged when the normalized residuals were less than 10^{-5} and subsequent iterations did not change the flow field results.

3.2. Population balance equation model

The analysis in this paper is restricted to pure breakage processes under the assumption of negligible drop coalescence (Simon et al., 2003). Under this assumption, the PBE for a batch system can be written as (Canu, 2005; Chen et al., 1998; Coulaloglou and Tavlarides, 1977)

$$\frac{\partial n(v,t)}{\partial t} = -g(v)n(v,t) + \int_v^\infty \beta(v,v')v(v')g(v')n(v',t)\,dv' \tag{1}$$

where $n(v,t)\,dv$ is the number of drops with volume in the range $[v, v+dv]$ per unit volume of the dispersion, $g(v)$ is the breakage rate representing the fraction of drops of volume v breaking per unit time, $v(v)$ is the number of daughter drops formed by breakage of a mother drop of volume v, and $\beta(v,v')$ is the daughter drop distribution function representing the probability of forming a daughter drop of size v from breakage of a mother drop of size v'. We model the high-pressure homogenizer as a well-mixed batch system in which the initial drop volume distribution is the measured distribution of the coarse pre-emulsion, and each pass corresponds to one dimensionless time unit. Our particle size analyzer provided measurements of the volume percent distribution $n_p(v,t)$ rather than the number density $n(v,t)$ as in PBE model (1). Consequently, the PBE model was reformulated in terms of volume percent distribution using the following relation based on the assumption of spherical drops consistent with experiments:

$$n(v,t) = \frac{V_{tot}n_p(v,t)}{v} \tag{2}$$

where V_{tot} is the conserved total volume of the drops. Simple manipulations produced the following alternative form of the PBE model:

$$\frac{\partial n_p(v,t)}{\partial t} = -g(v)n_p(v,t) + v\int_0^\infty \frac{g(v')v(v')\beta(v,v')n_p(v',t)}{v'}\,dv' \tag{3}$$

The PBE model (3) contains three breakage kernels ($g(v)$, $\beta(v,v')$, $v(v)$) that must be specified to generate predictions. To our knowledge, mechanistic functions are not available for the number of drops formed upon breakage $v(v)$ and the daughter drop distribution $\beta(v,v')$. Although the breakage of mother drops into multiple daughter drops has been reported by some investigators (Sathyagal and Ramkrishna, 1996; Vankova et al., 2007a; Tcholakova et al., 2007; Kostoglou and Karabelas, 2005), we have assumed binary breakage such that $v(v)=2$ for simplicity and to examine the possible limitations of assuming that multiple breakage events can be modeled as a series of binary breakage events. We further assumed that $\beta(v,v')$ follows the truncated normal distribution such that breakage has the highest probability of forming two equally sized daughter drops (Soon et al., 2001; Maguire et al., 2003; Ruiz and Padilla, 2004):

$$\beta(v,v') = \frac{2.4}{v'}\exp\left[-4.5\frac{(2v-v')^2}{(v')^2}\right] \tag{4}$$

We limited our consideration of the breakage rate $g(v)$ to two mechanistic functions that explicitly depend on the physical properties of the emulsion and allowed the resulting PBE models to account for chemical composition variations. The first function $g_1(v)$ is a modified version of two previously proposed functions (Chen et al., 1998; Coulaloglou and Tavlarides, 1977) which were derived assuming that breakage results from drop collision with turbulent eddies. Unlike the breakage function proposed by Chen et al. (1998), our function does not account for the small effect of the dispersed phase viscosity, but the breakage time t_B is assumed to be dependent on drop volume rather than being constant:

$$t_B = c_1 v^{2/9}\left(\frac{\varepsilon}{\rho_d}\right)^{-1/3} \tag{5}$$

The breakage function was specialized to high-pressure homogenizers by using the following relation between the energy dissipation rate ε and the homogenization pressure P (Becher, 1983a,b; Floury et al., 2004a,b; Walstra, 1993):

$$\varepsilon = c_2 P^{3/2} v^{-1/3}\rho_d^{-3/2} \tag{6}$$

Following the procedure in Chen et al. (1998), the following breakage rate function was derived:

$$g_1(v) = K_1 v^{-1/3}P^{1/2}\rho_d^{-1/2}\exp\left[-\frac{K_2\sigma(1+\phi)^2}{v^{1/3}P}\right] \tag{7}$$

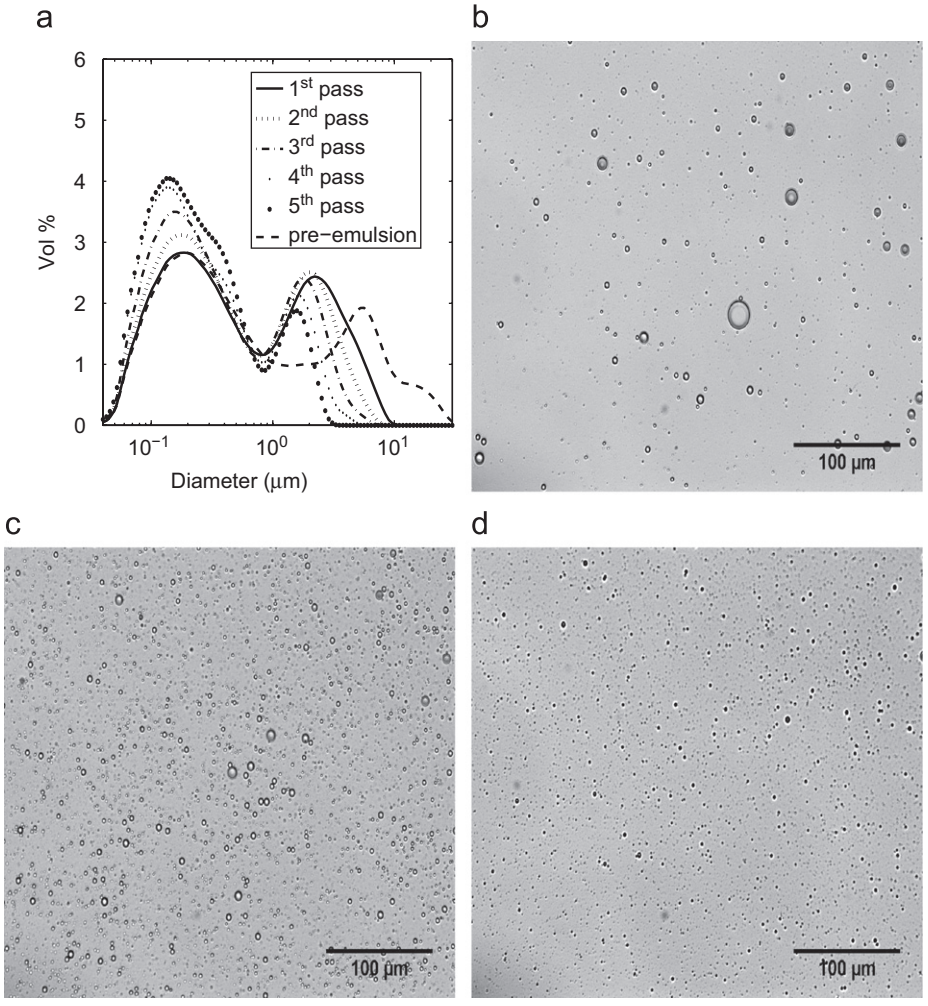

Fig. 1. (a) Measured drop volume distributions for the base case conditions. Optical microscopy image at 20× magnification of (b) the pre-emulsion, (c) the homogenized sample after the first pass, and (d) the homogenized sample after the fifth pass.

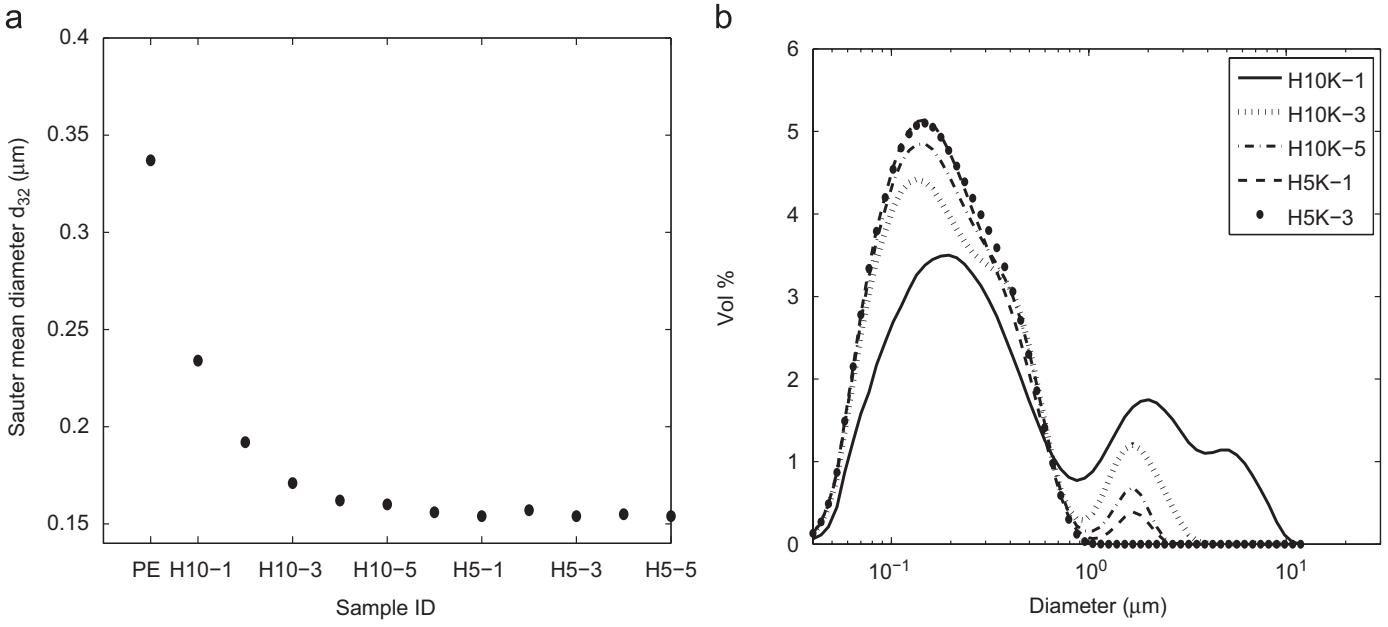

Fig. 2. Recoalescence test where the base case formulation was homogenized for six passes at 10 000 psig (labeled H10K-1 through H10K-6) and then homogenized for five passes at 5000 psig (labeled as H5K-1 through H5K-5). (a) Sauter mean diameters d_{32}. (b) Drop volume distributions.

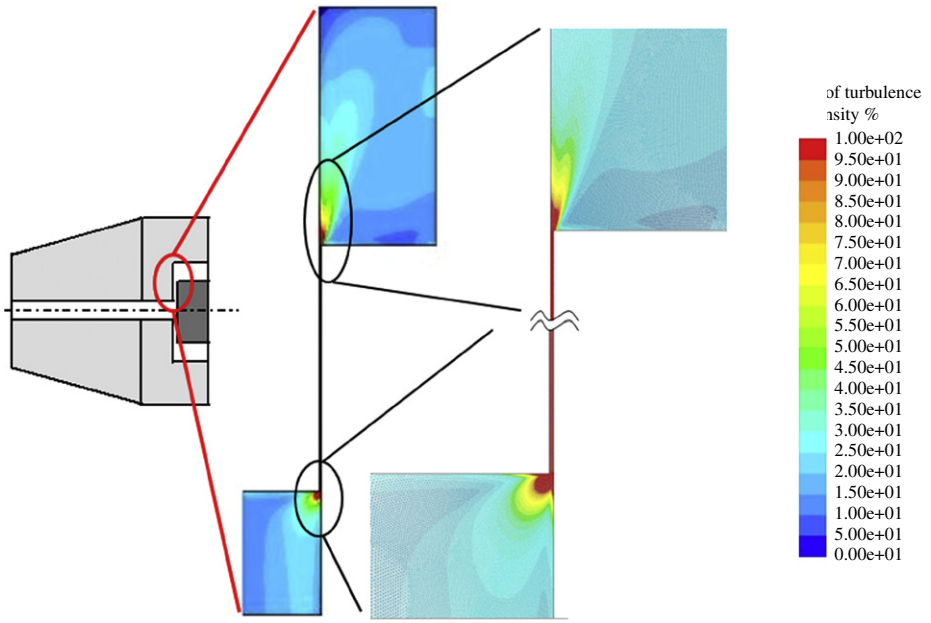

Fig. 3. Computational fluid dynamics simulation of the homogenizing valve gap showing contours of turbulence intensity (%) near the valve. The section of the homogenizing valve is shown at the extreme left. The portion of the valve gap used for CFD calculation is shown in the center. Enlarged sections of the gap inlet, the middle part of the gap, and the gap outlet are shown on the right.

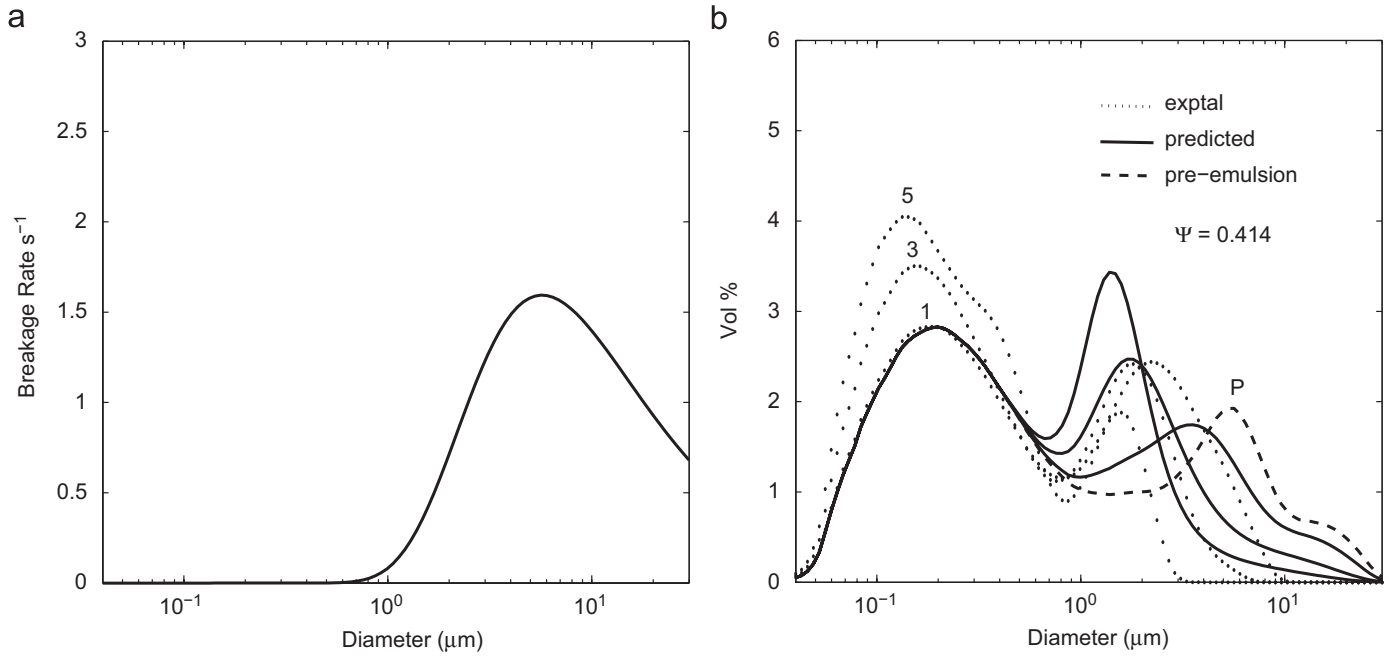

Fig. 4. Base case parameter estimation results with the drop-eddy collision breakage function $g_1(v)$. (a) Breakage rate. (b) Predicted and experimental drop volume distributions for the pre-emulsion (P), the first pass (1), the third pass (3), and the fifth pass (5). Ψ is the objective function value.

where K_1 and K_2 are parameters determined from measured drop size distributions (see below). Note that the breakage rate depends on the homogenizer pressure P and bulk emulsion properties including the dispersed phase volume fraction ϕ, the dispersed phase density ρ_d, and the interfacial tension σ.

The second breakage rate function $g_2(v)$ accounts for drop breakage resulting from turbulent shear. The derivation shown in the Appendix produces the following functional form:

$$g_2(v) = K_3\left(\frac{2}{\pi}\right)^{1/2}\left(\frac{P^{3/4}}{\eta_d^{1/2}\rho_d^{1/4}v^{1/6}}\right)\exp\left(\frac{-2K_4\sigma^2\lambda}{\eta_c P^{3/2}\rho_d^{-1/2}v^{1/3}}\right) \quad (8)$$

where $\lambda = \eta_d/\eta_c$ and K_3 and K_4 are adjustable constants. In addition to depending on the same emulsion properties as $g_1(v)$, the turbulent

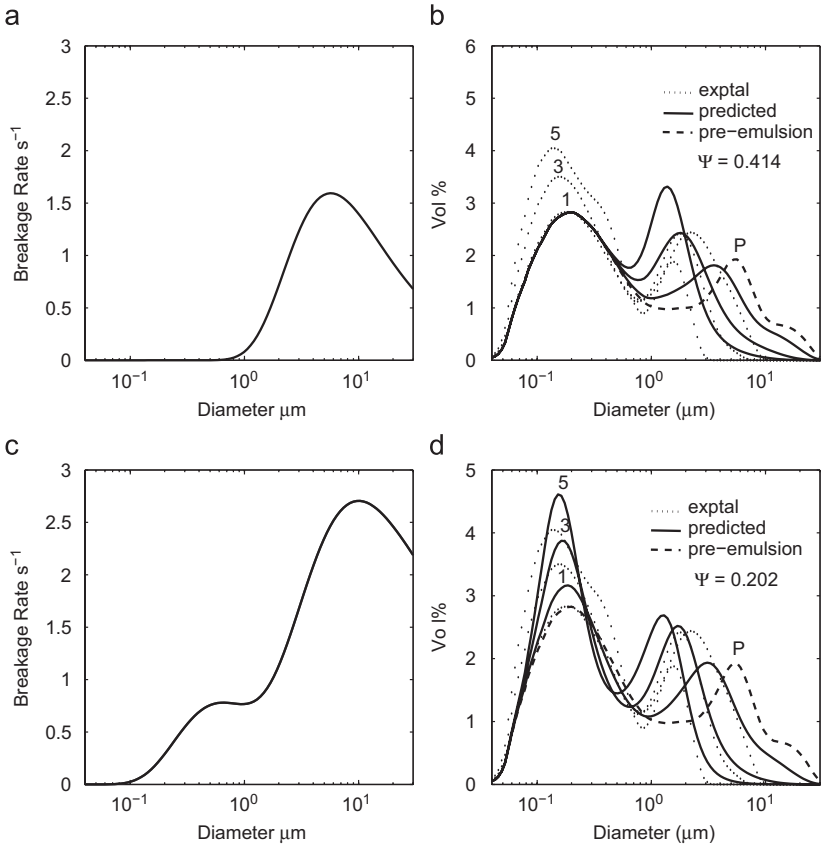

Fig. 5. Base case parameter estimation results with the shear breakage function $g_2(v)$. (a) Breakage rate. (b) Predicted and experimental drop volume distributions. Base case parameter estimation results with the combined breakage function $g(v) = g_1(v) + g_2(v)$. (c) Breakage rate. (d) Predicted and experimental drop volume distributions.

shear function $g_2(v)$ also depends on the continuous phase viscosity η_c and the dispersed phase viscosity η_d.

A variety of numerical techniques have been developed for solving PBE models of particulate processes (Kumar and Ramkrishna, 1996; Ramkrishna, 2000; Dorao and Jakobsen, 2006; Gavi et al., 2008). In this study, the PBE model (3) was solved numerically by approximating the integral expression using Simpson's rule with 100 equally spaced node points. The resulting system of 100 nonlinear ordinary differential equations describing the time evolution of the volume percent distribution at each node point was solved using the Matlab integration code `ode45`. The measured distribution of the coarse pre-emulsion was used as the initial condition $n_p(v, 0)$.

3.3. Parameter estimation

The constants K_1–K_4 in the breakage rate functions (7) and (8) were estimated from drop volume distribution measurements using a systematic nonlinear optimization procedure rather than an inefficient trial-and-error procedure. The data available for parameter estimation consisted of measured bulk emulsion properties $(\phi, \sigma, \rho_d, \eta_d, \eta_c)$ and drop volume distribution measurements for the coarse pre-emulsion $n(v, 0)$ and the processed emulsion obtained after the ith homogenizer pass $n(v, i)$. In addition to approximating the integral expression with Simpson's rule, the PBE model (3) was spatially and temporally discretized to produce a large set of nonlinear algebraic equations suitable for the application of constrained optimization codes. Spatial discretization in the volume space was performed using a finite difference approximation with 100 node points. Temporal discretization was performed using orthogonal collocation on finite elements where each pass corresponded to a single finite element and two internal collocation points were employed within each finite element. We found that additional spatial node points, finite elements, and/or collocation points had a negligible effect on the parameter estimates but increased the computational effort significantly.

The parameter estimation problem was posed as the constrained minimization of the following least-squares objective function:

$$\Psi = \sum_{i=1}^{N} \sum_{j=1}^{n} \frac{[\hat{n}_p(v_j, i) - n_p(v_j, i)]^2}{[n_p(v_j, i)]^2} \tag{9}$$

where $n_p(v_j, i)$ is the measured value of the drop volume distribution at drop volume v_j and homogenizer pass i, $\hat{n}_p(v_j, i)$ is corresponding predicted value from the PBE model (3), n is the total number of spatial node points, and N is the number of passes. The objective function was minimized subject to a large number of equality constraints representing the discretized model equations and continuity conditions across the finite elements. The decision variables in optimization problem were constants K_1 and K_2 if $g(v) = g_1(v)$, constants K_3 and K_4 if $g(v) = g_2(v)$, or the four constants K_1–K_4 if $g(v) = g_1(v) + g_2(v)$. The optimization problem was formulated in AMPL (Fourer et al., 2003) and solved using the nonlinear program code CONOPT. For some cases, multiple data sets were used and the objective function Ψ included a third sum over the data sets. Relative values of the objective function were used to judge the quality of model predictions.

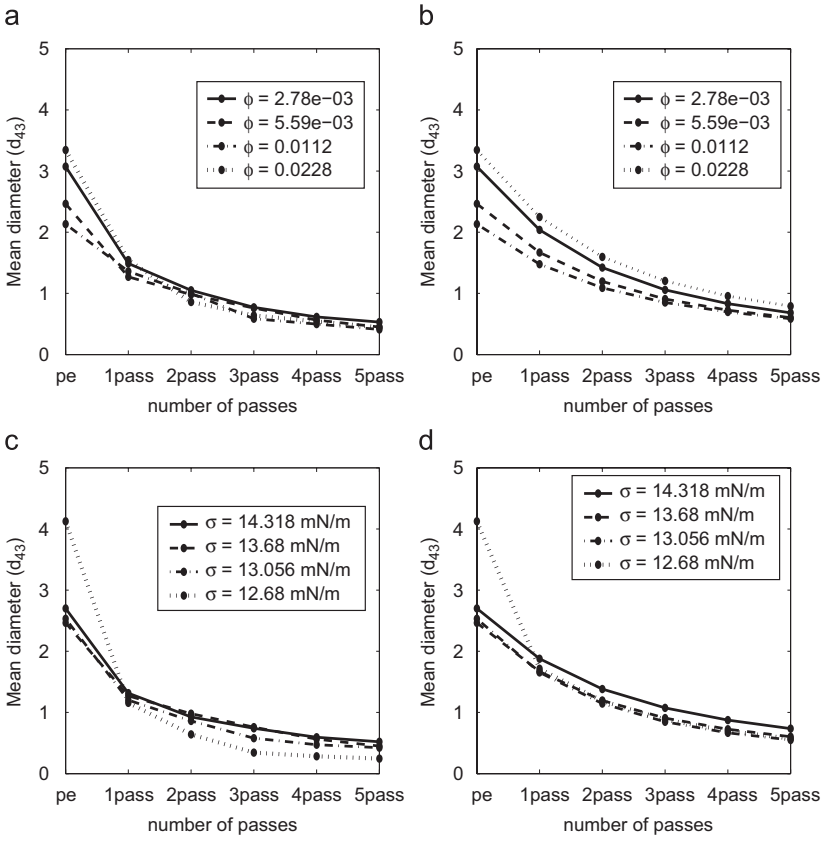

Fig. 6. Effect of dispersed phase volume fraction and interfacial tension on the experimental and predicted mean diameters. (a) Experimental mean diameters d_{43} for changes in dispersed phase volume fraction. (b) Predicted mean diameters d_{43} using base case values for changes in dispersed phase volume fraction. (c) Experimental mean diameters d_{43} for changes in interfacial tension. (d) Predicted mean diameters d_{43} using base case values for changes in interfacial tension.

4. Results and discussion

4.1. Homogenized drop volume distributions

We prepared five sample emulsions at the base case conditions (Table 1), performed five homogenization passes for each sample, and measured the drop volume distribution after each pass for each sample to analyze data reproducibility. The maximum standard deviation in the measured drop size distribution based on five repeats for any pass was about 9%, indicating that the experimental procedure and the distribution measurements were quite reproducible.

Fig. 1(a) shows a representative set of drop distribution measurements for the base case conditions. The pre-emulsion produced a bimodal distribution with the two peaks exhibiting large differences in drop diameter. Successive homogenizer passes had the effect of reducing the volume percentage of large drops, increasing the percentage of small drops, and sharpening the two peaks. The peak diameter of larger drops was noticeably reduced with successive passes, while the peak diameter of smaller drops remained roughly constant. Each pass produced a smaller relative change in the distribution, indicating that the breakage rate decreased with decreasing drop size. Fig. 1(b)–(d) show optical microscopy images at 20× magnification of the pre-emulsion, the first pass, and the fifth pass, respectively. The images were consistent with the measured drop distributions, with subsequent passes producing a larger fraction of small drops and all three samples having a noticeable bimodal nature.

4.2. Recoalescence test

The PBE model (3) used in this study is based on the assumption of negligible drop coalescence in the homogenizer. The term recoalescence is used to denote coalescence occurring in the homogenizer from newly formed drops. While the base case emulsion (Table 1) was formulated to have a low dispersed phase volume fraction and a high surfactant concentration to minimize recoalescence, we performed a targeted experiment to test this assumption. A base case emulsion was prepared and successively homogenized for six passes at 10 000 psig (68.95 MPa) until the Sauter mean diameter and drop distribution remained approximately constant, at which time the rates of drop breakage and drop coalescence (if present) were expected to be equal. The sample obtained after the sixth pass at 10000 psig was reprocessed with five additional passes at 5000 psig (34.47 MPa), which was expected to produce a reduced breakage rate and an increased coalescence rate if significant recoalescence was occurring. If the mean diameter and drop volume distribution remained approximately constant after successive passes at 5000 psig, then the coalescence rate was judged to be negligible relative to the breakage rate.

Fig. 2a and b shows the results of this experiment, with the six passes at 10 000 psig (68.95 MPa) labeled H10K-1–H10K-6 and the five passes at 5000 psig labeled H5K-1–H5K-5. Convergence of the Sauter mean diameters and the drop distributions support the assumption of negligible coalescence at the base case condition. While this assumption was not validated for the other conditions studied, we were confident that the coalescence rate remained

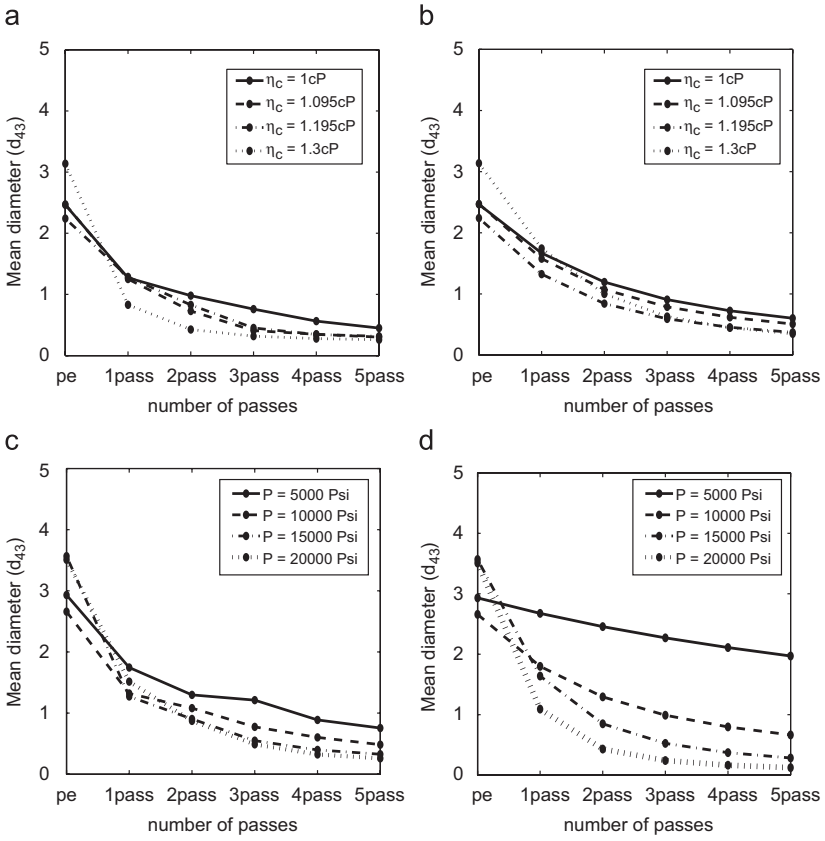

Fig. 7. Effect of continuous phase viscosity and pressure on the experimental and predicted mean diameters. (a) Experimental mean diameters d_{43} for changes in continuous phase viscosity. (b) Predicted mean diameters d_{43} using base case values for changes in continuous phase viscosity. (c) Experimental mean diameters d_{43} for changes in pressure. (d) Predicted mean diameters d_{43} using base case values for changes in pressure.

small. We also calculated the theoretical surface load from measured values of the interfacial tension versus surfactant concentration. The ratio of the adsorption to collision time scale (Walstra, 2003) shown below provides a qualitative measure of the extent of recoalescence

$$\frac{\tau_{ads}}{\tau_{coll}} = \frac{6\pi\Gamma\phi}{dC_s} \tag{10}$$

where Γ is the surface load and C_s is surfactant concentration. For negligible recoalescence, the ratio of τ_{ads}/τ_{coll} should be less than 1. At our base case conditions this ratio was in the range of 0.15–0.3, further indicating that recoalescence is negligible.

4.3. Computational fluid dynamics

Fig. 3 shows CFD results for the homogenizing valve and the truncated section near the valve that constituted the domain for flow field calculations. Although not included in our simple PBE model, the CFD calculations indicated strong spatial heterogeneities over the homogenizer domain. The contours demonstrated that the turbulence intensity was large in and at the exit of the valve gap and comparatively small elsewhere. Reynolds numbers in the range of 2000–4000 were calculated for most of the gap section, indicating the presence of a turbulent flow field. These results suggested that turbulence is an important mechanisms for drop breakage in the gap region and provided a mechanistic basis to apply the breakage rate functions (7) and (8) to our system.

4.4. Base case parameter estimation

We performed parameter estimation for the base case emulsion (Table 1) to better understand the relevant mechanisms for drop breakage. First parameter estimation was performed using the breakage rate function $g_1(v)$ (7) derived under the assumption that breakage results from drop collision with turbulent eddies. Measured drop volume distributions for the pre-emulsion and for the five processed emulsions sampled after each pass were used to estimate the unknown constant K_1 and K_2. Fig. 4(a) shows the resulting dependence of $g_1(v)$ on the drop diameter. The breakage function exhibited a maximum rate at a drop diameter of approximately 5 μm, suggesting reduced breakage for very large drops, and small breakage rates below 1 μm, indicating negligible breakage of small drops. The corresponding drop distribution predictions are shown in Fig. 4(b) along with the objective function value Ψ. The parameterized PBE model generated poor predictions, with the peak for larger drops poorly tracked and the movement of the peak for smaller drops not captured whatsoever due to the negligible breakage rates predicted at small drop sizes. The decreasing breakage rate above 5 μm appeared to have a relatively small effect on drop distribution predictions as the model emulsions had only a small number of such large drops.

Next parameter estimation was performed to determine constants K_3 and K_4 of the breakage rate function $g_2(v)$ (8) derived under the assumption that turbulent shear was the primary mechanism for drop breakage. The results (Fig. 5(a) and (b)) were very similar to those obtained for the other breakage function. The optimizer determined that the objective function Ψ was minimized by placing

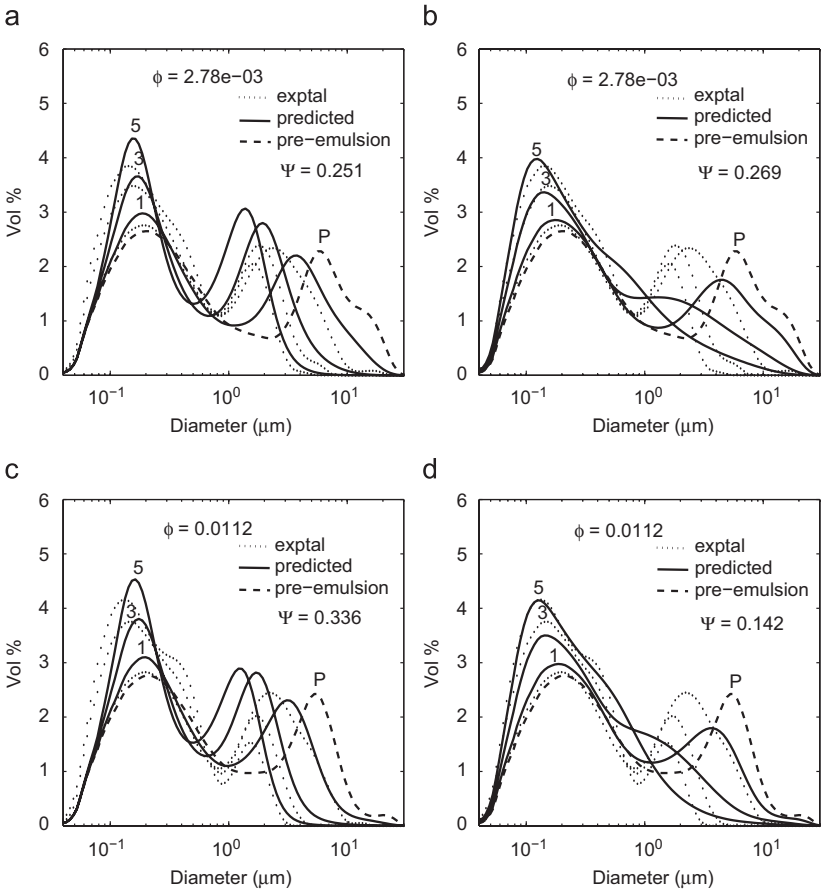

Fig. 8. Effect of the dispersed phase volume fraction on predicted drop volume distributions with the combined breakage function $g(\nu)$ for the pre-emulsion (P), the first pass (1), the third pass (3), and the fifth pass (5). Ψ is the objective function value. The base case values were used for the adjustable breakage parameters K_1–K_4. (a) $\phi = 2.78 \times 10^{-3}$. (c) $\phi = 0.0112$. The parameters K_1–K_4 were re-estimated using a combined data set containing the dispersed phase volume fraction variations. (b) $\phi = 2.78 \times 10^{-3}$. (d) $\phi = 0.0112$.

the breakage rate peak at a relatively large drop diameter due to the greater contribution of the large drop region to Ψ. As a result, very little breakage of small drops was predicted and the experimentally observed movement of the smaller drop peak could not be tracked. These results demonstrated that neither of two breakage rate functions alone could capture experimentally observed trends and suggested that some relevant physics were not modeled.

Although the large deviations observed between experimental and predicted drop distributions could be attributed to other factors, we investigated the possibility that the two turbulent breakage mechanisms were simultaneously active. For this case, the breakage rate function $g(\nu) = g_1(\nu) + g_2(\nu)$ and the four constants K_1–K_4 were estimated. We found that the optimizer could converge to two locally optimal solutions that produced identical Ψ values depending on the initial parameter guesses. Each solution produced a slightly bimodal breakage function, with the first peak for small drops corresponding to one function and the second peak for large drops corresponding to the other function. The solutions differed according to which function corresponded to which peak. Based on timescale arguments presented in Appendix B, we determined that the more physically meaningful solution was $g_1(\nu)$ representing the first peak and $g_2(\nu)$ representing the second peak (Fig. 5(c)). The combined breakage function produced much closer agreement to the experimental data (Fig. 5(d)) than either function alone, as reflected by the smaller Ψ value (0.202 versus 0.414 in Fig. 4(b)). The movement of both peaks in the drop distribution was qualitatively captured, although noticeable differences between the measured and predicted distributions remained. We judged these base case modeling results to be acceptable.

4.5. PBE model extensibility

We sought to investigate the extensibility of the PBE model with the combined breakage rate function to conditions other than the base case. The dispersed phase volume fraction (ϕ), the interfacial tension (σ), the continuous phase viscosity (η_c), and the homogenizer pressure (P) were varied from their base case values (Table 1) to determine if K_1–K_4 values estimated from the base case data could produce satisfactory drop distribution predictions over a range of conditions. For each case, the four parameters were also re-estimated from a combined data set that included variations in the associated emulsion property or the homogenizer pressure to determine if improved predictions could be generated.

First we compared experimental and predicted values of the De Brouckere mean moment diameter d_{43} (McClements, 2005) to determine if the PBE model could capture the general trends observed experimentally. The mean diameter d_{43}, which is defined as the ratio of the fourth moment over the third moment of the drop distribution, provides a meaningful scalar measure of the mean diameter for the bimodal distributions observed in our data sets. To investigate the effect of the dispersed phase volume fraction (ϕ), the oil concentration was reduced by 50% ($\phi = 2.78 \times 10^{-3}$) and increased by 200% ($\phi = 0.0112$) and 400% ($\phi = 0.0228$) from the base case

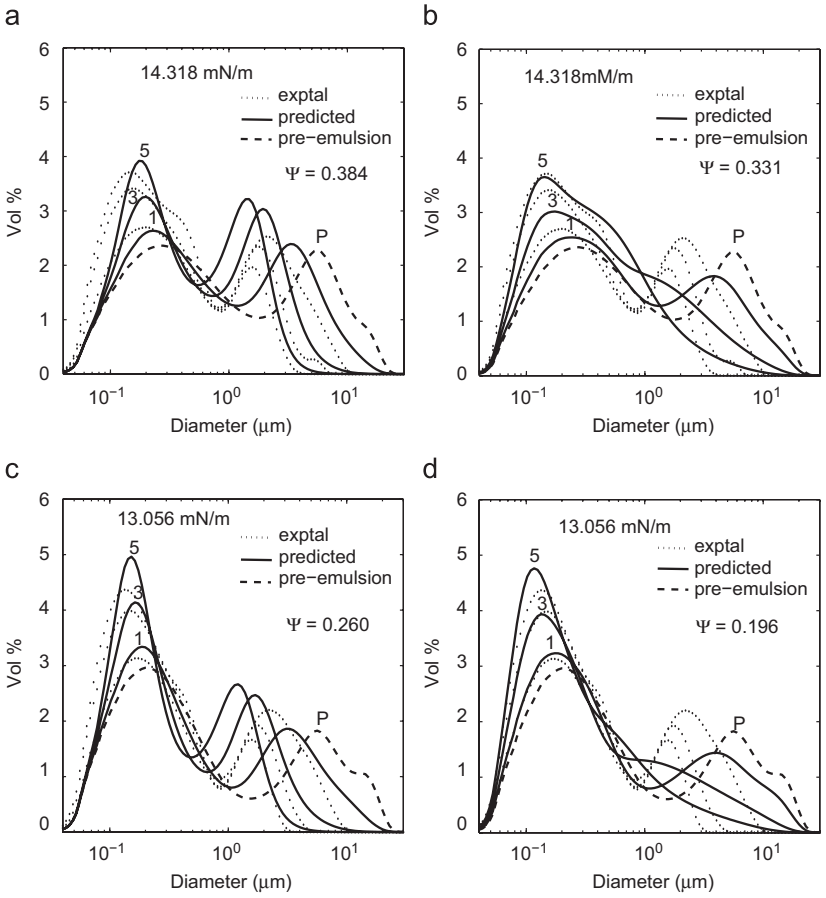

Fig. 9. Effect of the interfacial tension on predicted drop volume distributions with the combined breakage function $g(\nu)$. The base case values were used for the adjustable breakage parameters K_1–K_4. (a) $\sigma = 14.318$ mN/m. (c) $\sigma = 13.056$ mN/m. The parameters K_1–K_4 were re-estimated using a combined data set containing the interfacial tension variations. (b) $\sigma = 14.318$ mN/m. (d) $\sigma = 13.056$.

value ($\phi = 5.59 \times 10^{-3}$). The experimental (Fig. 6(a)) and predicted (Fig. 6(b)) results show good agreement, demonstrating that the model can capture trends in ϕ. The effect of the interfacial tension (σ) was examined by varying the surfactant concentration by 50% (σ=14.32 mN/m), 200% (σ=13.06 mN/m), and 300% (σ=12.68 mN/m) from the base case value ($\sigma = 13.68$ mN/m). The model (Fig. 6(d)) captured the decreasing mean diameter observed experimentally (Fig. 6(c)) for increasing surfactant concentration.

The continuous phase viscosity (η_c) was increased from its base value ($\eta_c = 1$ cP) by adding varying amounts of sucrose to the water. While the model (Fig. 7(b)) captured the decreasing mean diameter observed experimentally (Fig. 7(a)) for increasing continuous phase viscosity, the results for the largest value (η_c=1.3 cP) were only qualitatively correct. The homogenizer pressure (P) was varied over the range 5000–20 000 Psi (34.47–137.9 MPa), with the nominal value being $P = 10\,000$ Psi. The model (Fig. 7(d)) reproduced the experimental trend (Fig. 7(c)) that the mean diameter decreased with increasing pressure. However, the predicted results show significant errors, especially for the lowest pressure ($P = 5000$ Psi). Taken collectively, these results suggested that the functional dependencies of the combined breakage rate functions $g(\nu)$ was reasonable but that quantitative predictions with the base case model parameters may be difficult. Below we further examine this issue by analyzing results for the full drop size distribution.

4.5.1. Dispersed phase volume fraction

The base case dispersed phase volume fraction was reduced by half ($\phi = 2.78 \times 10^{-3}$) and doubled ($\phi = 0.0112$) by changing the oil concentration. Drop distributions predicted with the base case parameter values are compared to experimentally measured distributions in Fig. 8(a) and (c). Also shown are objective function Ψ values calculated directly from (9). For the reduced ϕ value, re-estimation of K_1–K_4 parameters did not provide any improvement in prediction accuracy (Fig. 8(b)). By contrast, re-estimation produced significant improvement for the increased ϕ value (Fig. 8(d)). We concluded that the functional dependence of the breakage rate on the dispersed phase volume fraction was reasonable, but that parameter estimation with data generated for varying ϕ would be necessary to more accurately predict the effect of this formulation variable.

4.5.2. Interfacial tension

The base case surfactant concentration was reduced by half and doubled, and the resulting changes in the interfacial tension σ were measured to be 14.32 and 13.06 mN/m, respectively. Comparison of predicted drop distributions obtained with the base case parameter values and experimentally measured distributions showed that the PBE model was better able to predict the effects of surfactant concentration increases (Fig. 9(a) and (c)). Re-estimation of the K_1–K_4 parameters produced small decreases in the objective function values at the expense of degraded distribution predictions at large drop diameters and eventual disappearance of model bimodality (Fig. 9(b) and (d)). We concluded that the PBE model satisfactorily accounted for surfactant concentration changes, but that parameter estimation with data generated for varying σ may not improve predictive capability with respect to this formulation variable.

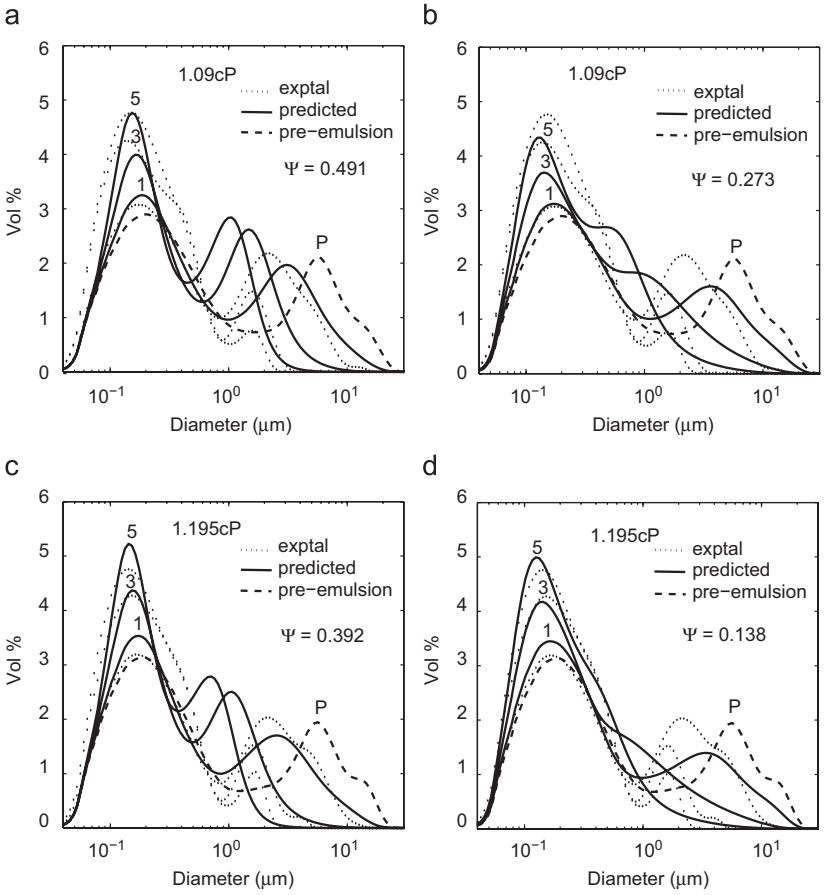

Fig. 10. Effect of the continuous phase viscosity on predicted drop volume distributions with the combined breakage function $g(v)$. The base case values were used for the adjustable breakage parameters K_1–K_4. (a) $\eta_c = 1.09$ cP. (c) $\eta_c = 1.195$ cP. The parameters K_1–K_4 were re-estimated using a combined data set containing the continuous phase viscosity variations. (b) $\eta_c = 1.09$ cP. (d) $\eta_c = 1.195$ cP.

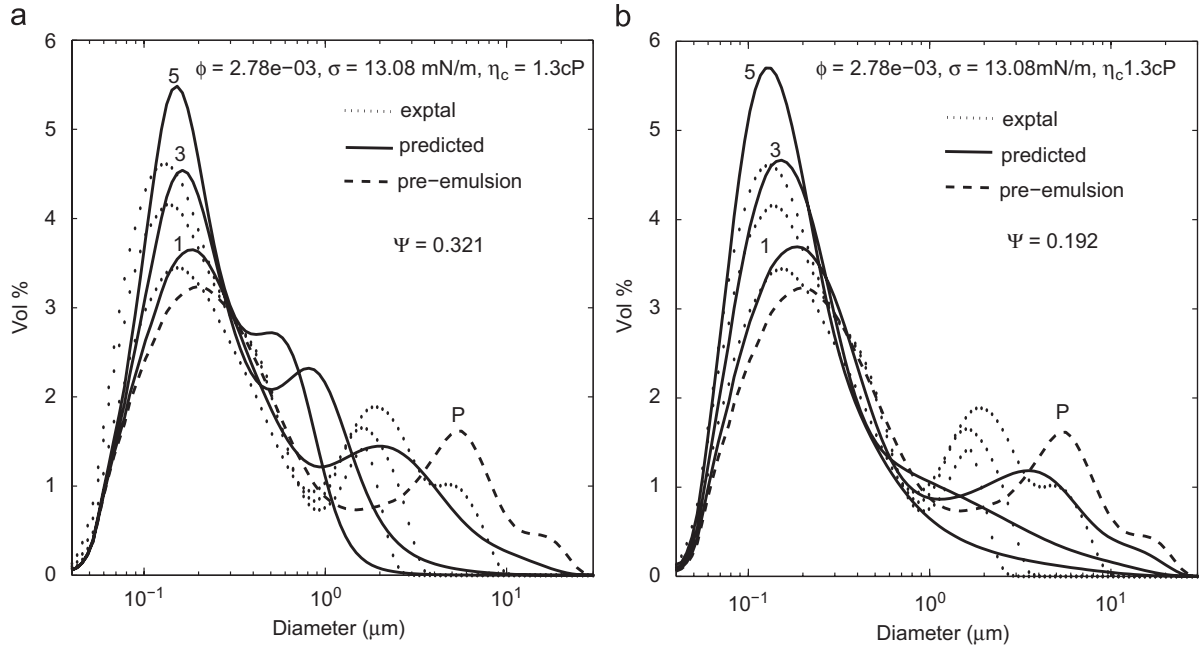

Fig. 11. Effect of simultaneous changes in the dispersed phase volume fraction, interfacial tension, and continuous phase viscosity with the combined breakage function $g(v)$. (a) The base case values were used for the adjustable breakage parameters K_1–K_4. (b) The parameters K_1–K_4 were re-estimated using a combined data set containing variations in the three formulation variables.

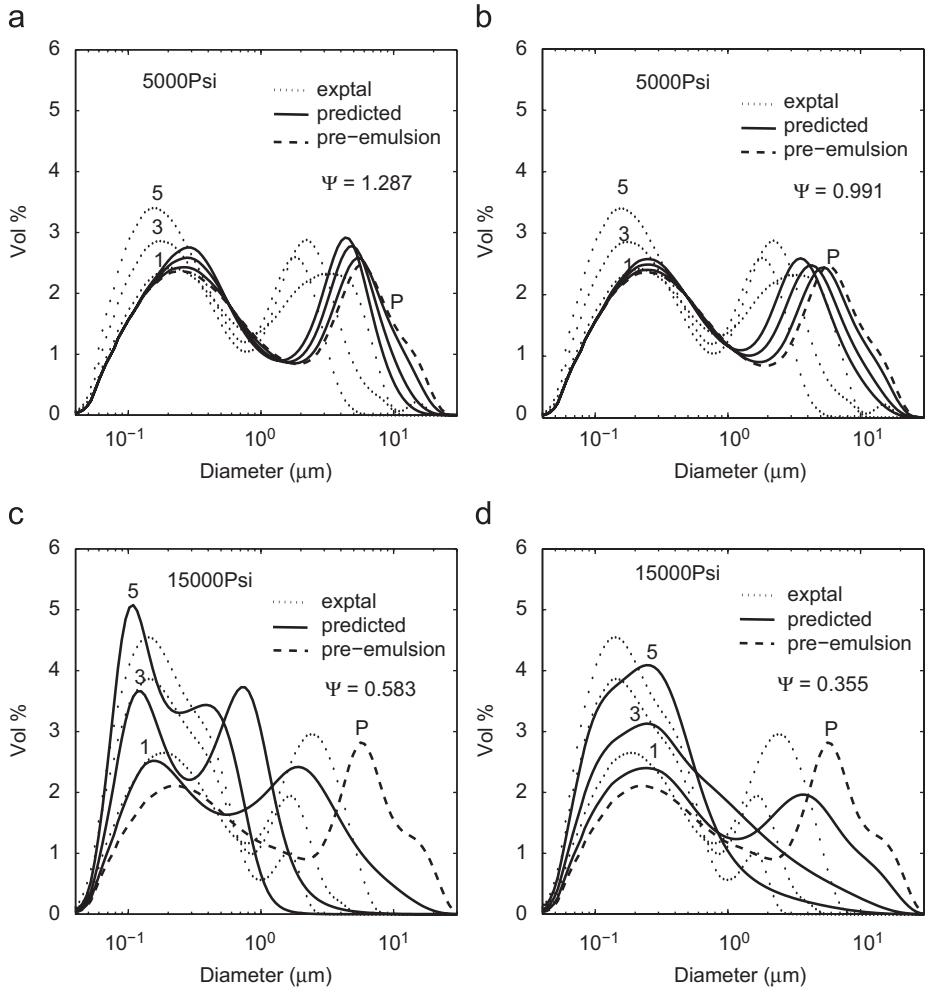

Fig. 12. Effect of the homogenization pressure on predicted drop volume distributions with the combined breakage function $g(\nu)$. The base case values were used for the adjustable breakage parameters K_1–K_4. (a) $P = 5000$ psig (34.47 MPa). (c) $P = 15\,000$ psig (103.42 MPa). The parameters K_1–K_4 were re-estimated using a combined data set containing the pressure variations. (b) $P = 5000$ psig (34.47 MPa). (d) $P = 15\,000$ psig (103.42 MPa).

4.5.3. Continuous phase viscosity

The continuous phase viscosity η_c was changed by adding varying amounts of sucrose to nanopure water used for emulsion preparation. Moderate and large additions of sucrose produced increased continuous phase viscosities of 1.09 and 1.195 cP, respectively, compared to the base case. The large sucrose addition also produced a slight change in interfacial tension, which was incorporated within the breakage rate function. Predicted drop distributions obtained with the base case parameter values are compared to experimentally measured distributions in Fig. 10(a) and (c). As measured by relative objective function values, the PBE model predictions showed larger deviations from data than observed for ϕ and σ variations. However, significantly improved predictions were obtained when K_1–K_4 parameters were re-estimated (Fig. 10(b) and (d)). We concluded that the functional dependence of the breakage rate on the continuous phase viscosity was reasonable, but that parameter estimation with data generated for varying η_c would be necessary to satisfactorily predict the effect of this formulation variable.

4.5.4. Multiple formulation variables

Rational design of emulsified products will require models capable of predicting the coupled effects of multiple formulation variables. To this end, we performed additional experiments in which the dispersed phase volume fraction, interfacial tension, and continuous phase viscosity were changed simultaneously from their base case values. Predicted drop distributions obtained with the base case parameter values are compared to experimentally measured distributions for a representative case in Fig. 11(a). The PBE model captured most of the qualitative trends with the exception of the predicted distributions approaching unimodality more quickly than the measured distributions. Re-estimation of K_1–K_4 parameters with a combined data set in which all the formulation variables were changed simultaneously produced a significant decrease in the objective function value (Fig. 11(b)), but the predicted distributions become unimodal even more rapidly than with the base case parameters. We concluded that the PBE model was capable of capturing the coupled effects of multiple formulation variables given an appropriate data set for parameter estimation.

4.5.5. Homogenization pressure

The homogenization pressure P was lowered to 5000 psig (34.47 MPa) and increased to 15 000 psig (103.42 MPa) from the base case value. Comparison of predicted drop distributions obtained with the base case parameter values and experimentally measured distributions showed that the PBE model was not able to satisfactorily capture pressure variations (Fig. 12(a) and (c)). Moreover, re-estimation of K_1–K_4 parameters with a combined data set in which the pressure was varied did not substantially improve the

model predictions (Fig. 12(b) and (d)). These results suggest that the pressure dependence of the energy dissipation rate (6) was incorrect. However, additional parameter estimation tests in which the pressure exponent in (6) was considered to be another adjustable parameter did not significantly improve the model predictions (not shown).

We believe that our CFD study may provide insights into this model deficiency. The turbulence intensity contours in Fig. 3 show strong spatial heterogeneities over the homogenizer domain, while the PBE model treats the homogenizer as a well-mixed system. Similar heterogeneities were observed in the pressure contours (not shown), with a large pressure drop from the valve gap inlet to the outlet. Accordingly, the assumption of a single homogenizer pressure is questionable and improved predictions over large pressure ranges may require the incorporation of spatial heterogeneities into the PBE model (Maguire et al., 2003).

5. Conclusion

We believe that the PBE modeling approach presented in this paper represents a necessary first step towards addressing the emulsion design problem for homogenized products. By invoking assumptions such as negligible drop coalescence, binary drop breakage, and homogeneous flow fields in the homogenizer, we investigated the ability of a simplified PBE model to match experimental data. Drop breakage functions that depend explicitly on formulation and processing variables were used such that the PBE model has the potential to reproduce qualitative trends in the drop volume distribution that result when these variable are changed. Consequently, the model can be used to predict the effects of different formulation properties before performing the associated experiments. This capability will not only allow new formulations to be identified but also will enable unacceptable solutions to be eliminated more rapidly and with less experimental effort. The current version of our PBE model does not adequately describe the effects of the homogenization pressure. Our future work will focus on better capturing the pressure effect, relaxing the assumption of binary breakage, including mechanistic descriptions of drop coalescence, and combining predicted drop distributions with physical property estimation techniques to allow the prediction of end-use characteristics.

Notation

c_1, c_2	constants
Ca	capillary number
Ca_c	critical capillary number
C_s	surfactant concentration, mg m^{-3}
d	drop diameter, m
$g(v)$	breakage rate of drops of size v, s^{-1}
G	shear rate, s^{-1}
G_b	critical shear rate, s^{-1}
K_1, K_2, K_3, K_4	adjustable parameters in breakage rate function $g(v)$
n	number of node points
N_{cp}	number of collocation points
$n(v,t)$	number of drops with size v per unit volume of the dispersion at time t
$n_p(v,t)$	volume percent distribution of drops of size v at time t
$\hat{n}_p(v_j,i)$	predicted volume percent distribution of drop of size v_j at ith pass
N	number of passes
P	operating pressure, Pa
t	time, s
t_B	breakage time, s
Δu	rms velocity difference, m s^{-1}
v	volume of drops, m^3
V_{tot}	total volume of drops, m^3

Greek symbols

$\beta(v,v')$	probability density function for daughter drops
Γ	surface load of the surfactant,mg m^{-2}
ε	local energy dissipation per unit volume, kg m^{-1} s^3
η_c	viscosity of continuous phase, Pa s
η_d	viscosity of dispersed phase, Pa s
λ	viscosity ratio
$\nu(v')$	number of daughter drops formed by breakage of a drop of size v'
ρ_d	density of dispersed phase, kg m^{-3}
ρ_c	density of continuous phase, kg m^{-3}
σ	interfacial tension, N m^{-1}
ϕ	volume fraction of the dispersed phase
Ψ	objective function defined in Eq. (9)

Subscripts

c	continuous phase
d	dispersed phase

Acknowledgments

We acknowledge financial support from the Petroleum Research Fund (Grant no. 44526-AC9), the National Science Foundation (Grant nos. 0730795 and DMI-0531171), and Unilever Foods. We would like to thank Prof. David Julian McClements (UMass Food Science) for providing access to particle size analyzers in his laboratory and to Prof. David Schmidt (UMass Mechanical and Industrial Engineering) for providing access to Fluent.

Appendix A. Derivation of the breakage rate function $g_2(v)$

The breakage rate is considered to be exponentially distributed as described by (Wang et al., 2005)

$$g(d) = \left(\frac{2}{\pi}\right)^{1/2} \frac{\Delta u}{d_i} \exp\left(\frac{-\Delta u_b^2}{\Delta u^2}\right) \tag{11}$$

where Δu is the rms velocity difference across distance d_i, and Δu_b is the critical velocity difference at which drop breakage occurs. The local shear rate is approximated as

$$G = \frac{\Delta u}{d_i} \tag{12}$$

Substituting for Δu and Δu_b yields

$$g(d) = \left(\frac{2}{\pi}\right)^{1/2} G \exp\left(\frac{-G_b^2}{G^2}\right) \tag{13}$$

where G_b is the critical shear rate that causes drop breakup. The Capillary number (Ca) for a drop of diameter d is given as

$$Ca_d = \frac{\eta_c G d}{2\sigma} \tag{14}$$

where η_c is the continuous phase viscosity, and σ is the interfacial tension. If $Ca_d > Ca_c$ (the critical capillary number), the drop is unstable and will eventually break. The critical shear rate can be written in terms of the critical capillary number Ca_c as (Dhingra, 2001)

$$G_b = \frac{2Ca_c\sigma}{\eta_c d} \tag{15}$$

Therefore, the breakage rate can be written as

$$g(d) = \left(\frac{2}{\pi}\right)^{1/2} G \exp\left(\frac{-(2Ca_c\sigma)^2}{(\eta_c G d)^2}\right) \tag{16}$$

For turbulent flow, G can be related to energy dissipation rate ε and the kinematic viscosity v (Marchisio et al., 2006; Wang et al., 2005). The resulting expression based on dispersed phase properties is

$$G = \sqrt{\frac{\varepsilon}{v}} = \sqrt{\frac{\varepsilon\rho_d}{\eta_d}} \tag{17}$$

Substituting for G in the breakage rate yields

$$g(d) = \left(\frac{2}{\pi}\right)^{1/2} \left(\frac{\varepsilon\rho_d}{\eta_d}\right)^{1/2} \exp\left(\frac{-(2Ca_c\sigma)^2\lambda}{(\eta_c d^2 \varepsilon\rho_d)}\right) \tag{18}$$

where $\lambda = \eta_d/\eta_c$ is viscosity ratio. Expressing ε in terms of pressure yields the final result

$$\varepsilon = \frac{c_1}{d}\left(\frac{P}{\rho_d}\right)^{3/2} \tag{19}$$

$$g(v) = g_2(v) = K_3\left(\frac{2}{\pi}\right)^{1/2} \left(\frac{P^{3/4}}{\eta_d^{1/2}\rho_d^{1/4}v^{1/6}}\right) \exp\left(\frac{-c_2(2Ca_c\sigma)^2\lambda}{\eta_c P^{3/2}\rho_d^{-1/2}v^{1/3}}\right) \tag{20}$$

This function depends on the pressure P, interfacial tension σ, dispersed phase density ρ_d, continuous phase viscosity η_c, dispersed phase viscosity η_d, and the critical capillary number Ca_c. The critical capillary number is expected to depend on the viscosity ratio and the type of flow (Gupta, 2004; Koper, 2007). However, for turbulent viscous flows the dependance on the viscosity ratio is not strong. Therefore, we invoke the assumption that Ca_c is constant and incorporate Ca_c into the adjustable constant K_4.

$$g(v) = g_2(v) = K_3\left(\frac{2}{\pi}\right)^{1/2} \left(\frac{P^{3/4}}{\eta_d^{1/2}\rho_d^{1/4}v^{1/6}}\right) \exp\left(\frac{-2K_4\sigma^2\lambda}{\eta_c P^{3/2}\rho_d^{-1/2}v^{1/3}}\right) \tag{21}$$

Appendix B. Appendix B

From turbulence theory, drops can break by collisions with turbulent eddies (function g_1) or due to viscous stress (function g_2). The size of the smallest eddy is given by (Hinze, 1955; Walstra, 1993, 2005; Vankova et al., 2007a; McClements, 2005)

$$\lambda_0 \approx \varepsilon^{-1/4}\eta_c^{3/4}\rho_c^{-1/2} \tag{22}$$

where ε is the energy dissipation rate per unit volume of fluid. The maximum stable drop size in the inertial turbulent regime is given by

$$d_i \approx \sigma^{3/5}\varepsilon^{-2/5}\rho_c^{-1/5} \tag{23}$$

For the case of shear or viscous turbulent flow, the maximum stable drop diameter is

$$d_v \approx \sigma\varepsilon^{-1/2}\eta_c^{-1/2} \tag{24}$$

For our base case conditions $d_v \approx \lambda_0 \approx d_i$, which implies that both inertial and viscous forces are important (Vankova et al., 2007a).

The deformation time scale is given by (Walstra, 1993, 2005)

$$t_{def} \approx \frac{\eta_d}{C\rho_c^{1/3}\varepsilon^{2/3}d^{2/3} - 4\sigma/d} \tag{25}$$

The lifetime of the eddy is

$$t_{eddy} \approx \frac{\rho_c^{1/3}d^{2/3}}{\varepsilon^{1/3}} \tag{26}$$

Because the deformation time is smaller than eddy lifetime for most of the size range considered, drops can be broken by inertial forces and viscous forces. Therefore, either function could be used to describe breakage at small drop sizes. Because d_v was larger than d_i, we used the turbulent eddy function (g_1) to describe breakup of small drops and turbulent shear function (g_2) to describe breakup of large drops.

References

Alopaeus, V., Koskinen, J., Keskinen, K., Majander, J., 2002. Simulation of the population balances for liquid–liquid systems in a nonideal stirred tank. Part 2—parameter fitting and the use of the multiblock model for dense dispersions. Chemical Engineering Science 57 (10), 1815–1825.

Becher, P., 1983a. Encyclopedia of Emulsion Technology, vol. I. Marcel Dekker, New York, NY.

Becher, P., 1983b. Encyclopedia of Emulsion Technology, vol. II. Marcel Dekker, New York, NY.

Becher, P., 2001. Emulsions: Theory and Practice. Oxford University Press, New York, NY.

Canu, P., 2005. Prediction of multimodal distributions in breakage processes. Industrial & Engineering Chemistry Research 44 (8), 2649–2658.

Chappat, M., 1994. Some applications of emulsions. Colloids and Surfaces A—Physicochemical and Engineering Aspects 91, 57–77.

Chen, Z., Pruss, J., Warnecke, H., 1998. A population balance model for disperse systems: drop size distribution in emulsion. Chemical Engineering Science 53 (5), 1059–1066.

Coulaloglou, C., Tavlarides, L., 1977. Description of interaction processes in agitated liquid–liquid dispersions. Chemical Engineering Science 32 (11), 1289–1297.

Dhingra, D., 2001. Feasible drop sizes in laminar emulsification systems. Master's Thesis, University of Massachusetts Amherst.

Dorao, C., Jakobsen, H., 2006. Numerical calculation of the moments of the population balance equation. Journal of Computational and Applied Mathematics 196 (2), 619–633.

Floury, J., Bellettre, J., Legrand, J., Desrumaux, A., 2004a. Analysis of a new type of high pressure homogeniser: a study of the flow pattern. Chemical Engineering Science 59 (4), 843–853.

Floury, J., Legrand, J., Desrumaux, A., 2004b. Analysis of a new type of high pressure homogeniser: part B: study of droplet break-up and recoalescence phenomena. Chemical Engineering Science 59 (6), 1285–1294.

Fourer, R., Gay, D.M., Kernighan, B.W., 2003. AMPL: A Modeling Language for Mathematical Programming. Brooks/Cole Publishing Company, Pacific Grove, CA.

Fluent Users Guide, 2005. Version 6.2. Fluent Inc, Lebanon, NH.

Gavi, E., Marchisio, D., Barresi, A., 2008. On the importance of mixing for the production of nanoparticles. Journal of Dispersion Science and Technology 29 (4), 548–554.

Gupta, S., 2004. Structured liquid products: emulsification process design for viscoelastic liquids. Master's Thesis, University of Massachusetts Amherst.

Hinze, J., 1955. Fundamentals of the hydrodynamic mechanism of splitting in dispersion processes. A.I.Ch.E. Journal 1 (3), 289–295.

Israelachvili, J., 1994. The science and applications of emulsions—An overview. Colloids and Surfaces A—Physicochemical and Engineering Aspects 91, 1–8.

Jaworski, Z., Pianko-Oprych, P., Marchisio, D., Nienow, A., 2007. CFD modelling of turbulent drop breakage in a kenics static mixer and comparison with experimental data. Chemical Engineering Research & Design 85, 753–759.

Kelly, W., Muske, K., 2004. Optimal operation of high-pressure homogenization for intracellular product recovery. Bioprocess and Biosystems Engineering 27 (1), 25–37.

Kim, J., Kramer, T., 2006. Improved orthokinetic coagulation model for fractal colloids: aggregation and breakup. Chemical Engineering Science 61 (1), 45–53.

Koper, G.J.M., 2007. An introduction to Interfacial Engineering. VSSD, Leeghwaterstraat, Delft, Netherlands.

Kostoglou, M., Karabelas, A., 2005. Toward a unified framework for the derivation of breakage functions based on the statistical theory of turbulence. Chemical Engineering Science 60 (23), 6584–6595.

Kumar, S., Ramkrishna, D., 1996. On the solution of population balance equations by discretization 1. A fixed pivot technique. Chemical Engineering Science 51 (8), 1311–1332.

Lander, R., Manger, W., Scouloudis, M., Ku, A., Davis, C., Lee, A., 2000. Gaulin homogenization: a mechanistic study. Biotechnology Progress 16 (1), 80–85.

Maguire, L., Zhang, H., Shamlou, P., 2003. Preparation of small unilamellar vesicles (SUV) and biophysical characterization of their complexes with poly-l-lysine-condensed plasmid DNA. Biotechnology and Applied Biochemistry 37, 73–81.

Marchisio, D., Soos, M., Sefcik, J., Morbidelli, M., 2006. Role of turbulent shear rate distribution in aggregation and breakage processes. A.I.Ch.E. Journal 52 (1), 158–173.

McClements, D.J., 2005. Food Emulsions: Principles, Practice, and Techniques. CRC Press, Boca Raton, FL.

Miller, J., Rogowski, M., Kelly, W., 2002. Using a CFD model to understand the fluid dynamics promoting e-coli breakage in a high-pressure homogenizer. Biotechnology Progress 18 (5), 1060–1067.

Nasr-El-Din, H.A., 1992. Fluid Dynamics in Oil–Water–Sand Systems in Emulsions: Fundamentals and Applications in the Petroleum Industry. American Chemical Society, Washington, DC.

Pal, R., Yan, Y., Masliyah, J., 1992. Rheology of Emulsions, in Emulsions: Fundamentals and Applications in the Petroleum Industry. American Chemical Society, Washington, DC.

Raikar, N.B., Bhatia, S.R., Malone, M.F., Henson, M.A., 2006. Self-similar inverse population balance modeling for turbulently prepared batch emulsions: sensitivity to measurement errors. Chemical Engineering Science 61 (22), 7421–7435.

Ramkrishna, D., 2000. Population Balances: Theory and Applications to Particulate Processes in Engineering. Academic Press, New York, NY.

Rimmer, D.P., Gregoli, A.A., Hamshar, J.A., Yildirim, E., 1992. Pipeline Emulsion Transportation for Heavy Oils, in Emulsions: Fundamentals and Applications in the Petroleum Industry. American Chemical Society, Washington, DC.

Ruiz, M., Padilla, R., 2004. Analysis of breakage functions for liquid–liquid dispersions. Hydrometallurgy 72 (3–4), 245–258.

Saniere, A., Henaut, I., Argillier, J., 2004. Pipeline transportation of heavy oils, a strategic, economic and technological challenge. Oil and Gas Science and Technology—Revue De L Institut Francais Du PetrolE 59 (5), 455–466.

Sathyagal, A., Ramkrishna, D., 1996. Droplet breakage in stirred dispersions: breakage functions from experimental drop-size distributions. Chemical Engineering Science 51 (9), 1377–1391.

Sathyagal, A., Ramkrishna, D., Narsimhan, G., 1995. Solution of inverse problems in population balances 2: particle break-up. Computers and Chemical Engineering 19 (4), 437–451.

Schramm, L.L., 1992. Petroleum Emulsions: Basic Principles in Emulsions: Fundamentals and Applications in the Petroleum Industry. American Chemical Society, Washington, DC.

Simon, M., Schmidt, S., Bart, H., 2003. The droplet population balance model-Estimation of breakage and coalescence. Chemical Engineering & Technology 26 (7), 745–750.

Soon, S., Harbidge, J., Titchener-Hooker, N., Shamlou, P., 2001. Prediction of drop breakage in an ultra high velocity jet homogenizer. Journal of Chemical Engineering of Japan 34 (5), 640–646.

Tcholakova, S., Vankova, N., Denkov, N., Danner, T., 2007. Emulsification in turbulent flow: 3. Daughter drop-size distribution. Journal of Colloid and Interface Science 310 (2), 570–589.

Vankova, N., Tcholakova, S., Denkov, N., Ivanov, I., Vulchev, V., Danner, T., 2007a. Emulsification in turbulent flow—1. Mean and maximum drop diameters in inertial and viscous regimes. Journal of Colloid and Interface Science 312 (2), 363–380.

Vankova, N., Tcholakova, S., Denkov, N., Vulchev, V., Danner, T., 2007b. Emulsification in turbulent flow 2. Breakage rate constants. Journal of Colloid and Interface Science 313 (2), 612–629.

Walstra, P., 1993. Principles of emulsion formation. Chemical Engineering Science 48 (2), 333–349.

Walstra, P., 2003. Physical Chemistry of Foods. Marcel Dekker, New York, NY.

Walstra, P., 2005. Emulsions. In: Lyklema, J. (Ed.), Fundamentals of Interface and Colloid Science: Soft Colloids. Elsevier, Academic Press, London.

Wang, L., Marchisio, D., Vigil, R., Fox, R., 2005. CFD simulation of aggregation and breakage processes in laminar Taylor–Couette flow. Journal of Colloid and Interface Science 282 (2), 380–396.

Woo, X., Tan, R., Chow, P., Braatz, R., 2006. Simulation of mixing effects in antisolvent crystallization using a coupled CFD–PDF–PBE approach. Crystal Growth & Design 6 (6), 1291–1303.

Yaghi, B., Al-Bemani, A., 2002. Heavy crude oil viscosity reduction for pipeline transportation. Energy Sources 24 (2), 93–102.